Comparing the broadband acoustic frequency response of single, clustered and arrays of marine air guns

by

M. Landrø[1]

[1]*NTNU, 7491 TRONDHEIM, NORWAY*

ABSTRACT

Field data acquired from a seismic vessel by a seabed hydrophone is used to analyze the broadband response (10 Hz to 62.5 kHz) for various source configurations: Single air guns, clustered air guns and a full array consisting of 30 air guns. The various parts of the acoustic signal is analyzed in detail, and it is found that a high frequency signal arriving prior to the main peak of a single air gun signal is most likely caused by small vapor cavities collapsing at or close to the surface of the gun. This is confirmed by high speed photographs taken when a small air gun is fired in a water tank. When the full array is used, a second type of cavitation signal is observed: Ghost cavitation caused by acoustic stimulation by the negative pressure that is backscattered from the free surface. As this ghost signal from 30 different guns arrive at a specific location in the water, cavities might be formed, and create a high frequency acoustic signal.

I. INTRODUCTION

In this work, I study source signatures of single air guns and a marine air gun array recorded by a far field hydrophone with a frequency bandwidth of 10 Hz to 62.5 kHz. The hydrophone was located vertically below the source at the seabed. Traditionally, the major interest for air gun performance has been to model and measure the emitted acoustic signals within the seismic bandwidth, which is between 5 and 250 Hz. For

marine seismic acquisition, air guns are the most commonly used sources. A brief introduction to air guns can be found in Dragoset (2000). The first example of air gun modeling was presented by Ziolkowski (1970). Later examples of modeling of air guns can be found in Landrø (1992) and Barker and Landrø (2014).

Recently, the interest for high frequency signals produced by air gun arrays has increased (Goold and Fish, 1998), (Breitzke et al., 2008), and (Amundsen and Landrø, 2011). (Amundsen and Landrø, 2010), discuss and present hearing curves of marine mammals. Both dolphins and white whales have excellent hearing capacity for frequencies between 10 and 100 kHz. Groenaas et al. (2011) suggests to include a high-frequency streamer section in a normal streamer for the purpose of detecting marine mammals.

Landrø et al., 2011 discuss the frequency properties and possible causes for the high frequency signals. They suggest that the mechanism of ghost cavitation can cause a significant amount of high frequency signals emitted from an air gun array. The more guns and the closer they are, the more the ghost cavitation effect will contribute to the high frequency signals. In another paper Landrø et al. (2013), discuss repeatability issues related to these signals, and conclude that both the amount and the timing related to the main peak are repeatable.

In this paper, the focus is on how single air guns contribute to the high frequency signals produced, and how the high frequency signals emitted by single guns compare to that of a big air gun array. What are the mechanisms behind such effects, and how strong is the high frequency signals from single air guns compared to a compact full

array of guns? Can we use superposition, and assume that the amount of high frequency signal created by a full array is the sum of each individual gun? The ghost cavitation hypothesis does not support such a linear superposition, simply because the ghost cavitation mechanism needs that the ghost signal is above a certain threshold before it is activated. In other words: An array of 3-4 small air guns might not produce ghost cavitation signals at all, in contrast to a bigger array. Recently Coste et al., 2014 presented a new air gun where the amount of high frequency signals is attenuated. By changing the design of the air gun, they show that the signal between 100 Hz and 6 kHz is reduced by approximately 10 dB by using the new air gun. From 7 to 10 kHz the new air gun spectrum is slightly above the conventional, but essentially there are no major differences between the new and the conventional air gun above 7 kHz. In this paper, I will discuss conventional air guns only. I analyze and suggest some mechanisms for high frequency emission from single and multiple air guns used for marine seismic imaging. I find that the amplitude level of the high frequency signals (above 10 kHz) is small compared to conventional seismic amplitudes, typically 60 dB lower.

II. THE FIELD EXPERIMENT

The field test was performed in the Black Sea offshore Turkey in December 2008. The shooting vessel was M/V Marlene Østervold, and several configurations of the source array were tested. The high frequency data were recorded by an electrical hydrophone located at the sea bottom, measuring frequencies up to 62.5 kHz (0.008 ms sampling rate). For each line, approximately 40 shots were shot as the ship was sailing on a straight line crossing over the sea bottom hydrophone. The water depth in the area is varying between 50 and 60 m. In this paper, I analyze data from four different source configurations: P09, P13, P14 and P19. P09 is a single 70 cubic inch air gun, P13 is a single 300 cubic inch air gun, P14 is a cluster of two 300 cubic inch air guns, and P19 is

the full array (2730 cubic inches). For the full array, the distance between the gun strings is 6 m, and the total number of guns in the array is 30. The source depth is 5 m for all shots used in this paper, and a detailed description of the gun array can be found in Landrø et al. (2013). The precise position of the sea bottom hydrophone relative to the source array is not known. However, from typical move out curves it is possible to find shots that are close to being straight above the hydrophone. For the present analysis, this lack of precise geometry information does not create severe problems.

III. DESIGN OF AIR GUNS AND POSSIBILITIES FOR CAVITY CREATION

Figure 1 shows a small BOLT air gun that has been cut to show the interior of the gun. When the gun is fired, a small amount of air is released from the upper gun chamber and the piston or shuttle starts to move upwards so that air from the lower (and bigger) chamber is released through the ports directly into the water surrounding the gun.
The size of the ports of air guns with different volumes are normally the same, one replaces the gun chamber and keeps the rest of the air gun unchanged when the gun volume is changed. A simple and well known equation often used to describe oscillating cavities or air bubbles is the Rayleigh (1917) equation:

$$R\ddot{R} + \tfrac{3}{2}\dot{R}^2 = \frac{p_B - p_h}{\rho} \qquad (1)$$

Where R is the bubble radius, p_B is the bubble pressure, p_h the hydrostatic pressure surrounding the bubble and ρ is the water density. Dot denotes time derivative. An obvious weakness of equation 1 is that the basic assumption is that the flow is radial and that we assume spherical symmetry. This is not the case when compressed air is released through the port openings of an air gun (Figure 1). At the early stages, there is actually four air bubbles (that later merge into one big bubble), and the fluid flow close to these four bubbles is not purely radial. Despite this, the Rayleigh equation gives a

reasonable estimate of how the bubble radius and bubble wall velocity varies with time. The probability of cavity creation is closely linked to abrupt changes in water velocity close to the gun. Typically, cavities will form at edges and corners at the gun itself, since the largest velocity gradients are likely to occur there. In principle, we expect more cavitation the faster the water initially surrounding the air gun (including the small volume inside the ports) moves outwards. Figure 2 shows a numerical solution of equation 1 assuming that the initial bubble pressure is 137 bar, and that the bubble radius is that corresponding to the gun volume. We notice that there is hardly any difference between the maximum bubble wall velocity for the two gun volumes (70 and 300 cubic inches), and hence we cannot conclude that the bigger gun creates more cavities than the smaller gun.

However, if we consider that the air has to escape through narrow ports, the situation is somewhat different. A simple, but far from very accurate way to model this is to use equation 4 in Landrø et al. (1993):

$$\left[p_0 \left(\frac{V_0}{V_0 + Az} \right)^{\gamma} - p_h \right] A = m\ddot{z}\,, \qquad (2)$$

where p_0 is the initial gun firing pressure, A is the area of the gun port, z is the position of the shuttle, m is the mass of the shuttle, V_0 is the initial gun volume and γ is the adiabatic constant (1.4 for air). Equation 2 is derived for a water gun, where compressed air is used to push a shuttle so that water is quickly pushed into the sea water, creating big cavities that collapse and create the acoustic signal of a water gun. In our case we have to assume that the water (that is initially in the area between the port openings and the core of the shuttle (Figure 1) escaping through the ports of the air gun acts like a piston on the water that is outside the gun ports. The mass of such a "water piston" is relatively low (probably less than 1 kg) and this number should be

divided by four since we have four ports where this water has to be pushed through at the initial stage after the gun has been fired. Using m = 0.25 kg in equation 2 and A = 0.0005 m^2, we can estimate the velocity of the water escaping through the ports during the first milliseconds. Since the gun has four ports, we have to correct for this in the volumetric term within the parenthesis in equation 2, and modify it to:

$$\left[p_0 \left(\frac{V_0}{V_0 + 4Az} \right)^{\gamma} - p_h \right] A = m\ddot{z} \,. \qquad (3)$$

Equation 3 describes the motion of a one “water piston” escaping from one port assuming that the mass is equal to the total mass of water that has to be moved out of the gun ports prior to the compressed air. Figure 3 shows the modelled water velocity through the ports using equation 3, and we observe that the largest gun volume gives somewhat higher water velocity. In the modelling the following parameters have been used: m = 0.25 kg, p_0 = 137 bar p_h = 1.5 bar, A = 0.0005 m^2. Both velocities are higher than those estimated directly from the high speed photography (50 m/s, see next section). This is reasonable since equation 3 is far from accurate: For instance there is no friction term in this equation and it is not describing the physics of pushing water through a nozzle correctly. However, it is reasonable to assume that the qualitative difference with respect to volume that is modelled from this equation is correct, and in this paper, this is the main purpose of this equation: To find out if it is likely that the water velocity will increase with increasing gun volume or not. An alternative argument supporting higher water velocities for larger gun volumes is that when the potential energy contained in the lower gun chamber (p_0V_0) increases there is more energy available to quickly remove the water that is inside the port openings prior to firing the gun. This water has to be removed and it is very likely that the kinetic energy associated

with the motion of this water increases if the potential energy pushing this water increases.

IV. HIGH SPEED PHOTOGRAPHY OF A SMALL AIR GUN IN A TANK

Langhammer and Landrø (1996) presented high speed photographs of a small (1.6 cubic inches) air gun that was fired in a water tank. This is the same type of gun that is shown in Figure 1. Figure 4 shows four such photographs taken at various time intervals. On the first photo (a) we observe that there is a small amount of air being released from the upper gun chamber (through a narrow opening in the air gun). This very tiny air bubble is probably causing the “shoulder signal” or precursor of the air gun acoustic signature (Figure 8). Furthermore, we do not see any sign of the air escaping from the main chamber (the lower chamber) on this photo, which means that the air has not started to move through the ports yet. We also observe some small bubbles attached to the upper ring of the air gun (above the ports). This is probably small air bubbles originating from a small leakage of air from the lower gun chamber. On the next photo (b) we clearly observe that some air is visible inside the gun, ready to escape through the port openings. Here some of the small bubbles on the upper ring are interpreted as vapor cavities. This is based on visual observation of the high speed video where these “bubbles” seems to be coupled to the rapid movement of water, and not the slower movement of leaking air bubbles. In c) we clearly see that the air has escaped through the ports. This means that the air has moved several centimeters within 0.3 ms (time interval between frame b and c). The distance from the thickness of the port opening is approximately 1 cm, and an estimate of the distance travelled by the air front between b) and c) is approximately 1.5 cm. A rough estimate for the average velocity of the air-water surface is therefore 0.015m/0.0003s = 50 m/s, which is significantly above the threshold for cavity production. In Langhammer and Landrø

(1996) we compared modeled and estimated bubble wall velocities for this small air gun and found similar numbers for the maximum velocity (40 m/s). It should be noted that there are significant uncertainties coupled to this type of velocity estimation: First of all there is an uncertainty in the number 0.3 ms (time delay between frame b and c). The distance traveled has also some uncertainty, although we clearly see from the pictures and direct measurements on the air gun that it is of the order of 1.5 cm. The threshold for cavity creation is given as (assuming a depth of 5 m; Landrø et al., 1993)

$$u_c = \sqrt{\frac{2p_h}{\rho}} \approx \sqrt{\frac{3\cdot 10^5}{10^3}} m/s = 17.3 m/s\,, \qquad (4)$$

which is far below the velocity estimated from the high speed photography. We notice that the threshold velocity increases with depth. This means that it is very likely that cavities are formed close to the port openings of an air gun. On the last photo (Figure 4d) we observe that the four bubbles emerging from each of the four gun ports start to merge, and that the size of these bubbles is growing. A rough estimate of the bubble wall velocity based on comparison of photo c) and d) in this series is 2 cm per 0.5 ms corresponding to 40 m/s. Figure 4b shows potential water vapour cavities (marked by white arrows). Note that these cavities occur on the metal right above the gun ports, and not below. A possible explanation for this is that the air is escaping towards the water surface (the piston or shuttle is also moving upwards) so the largest water velocities will occur right above the port openings, and hence cavities will be “glued” to the area right above the port openings. We also notice that there are some cavities on the ring above the port, however, the number of such cavities are less than those in the close vicinity to the gun ports. The size of these cavities is (estimated from Figure 4) between 1 and 4 mm. Using Rayleigh’s (1917) equation for the collapse time of a cavity with an assuming an initial radius *R=1* mm we get:

$$\tau = 0.915R\sqrt{\frac{\rho}{p_h}} \approx 0.02ms\,, \qquad (5)$$

which means that these small cavities will collapse within a very short time frame, and most likely less than 0.1 ms.

Another interesting observation from Figure 4 is that the small bubble or mini bubble grows in a more moderate speed compared to the big bubble that escapes from the big chamber of the air gun. The small bubble escapes through a small nozzle that has a diameter of the order of 1-2 millimetres. This is the main explanation for this difference in growing velocity between the two air bubbles. These two bubbles probably merge into one after 2 ms. The next question is whether we can detect the acoustic signal generated by cavities collapsing close to the air gun, and measured at a distance of 60 m below the gun.

V. ACOUSTIC SIGNALS FROM SINGLE AIR GUNS

Figure 5 (top) shows recorded acoustic signals for 3 shots representing a single 70 cubic inch air gun, a single 300 cubic inch air gun and a cluster of two 300 cubic inch air guns. We notice that the cluster has a maximum peak that is almost the double of the single gun. Furthermore, we notice that there are small ripples on all signatures, both prior to and during the main peak signal. Some of these ripples are high frequency signals created by the gun and some are background high frequency noise. This issue will be further addressed in later sections. The smallest gun (70 cubic inch) is a slightly different type (Bolt 1900 C) while the bigger guns are of type Bolt 1500 C. In this figure the closest shots (with respect to the hydrophone) have been chosen, and it is assumed that the distance from the source to the sea bed hydrophone is 60 m for all shots. As discussed above, there might be a slight variation in this distance, since the surface position for the nearest shot might vary by up to 15 m. To convert the signals to bar-m I

have simply multiplied the recorded signals by 60. Typical relative errors in amplitudes caused by this inaccuracy might be up to 3 %. The timing of the maxima for each shot is also somewhat random (5-10 ms spread), and these variations have been adjusted for in Figure 5 so that the rise of the main peak is aligned for various shots.

A detailed comparison of the “shoulder signal” (the signal prior to the main peak) is displayed in Figure 5 (bottom). We notice that the length of this signal is significantly longer for the 300 cubic inch air gun (44-48 ms) compared to the 70 cubic inch air gun (46-48 ms). This might be due to the fact that the two guns are of different types (Bolt 1500 C and 1900 C). The volume of the upper chamber for the big air gun (300 cubic inch, 1500 C) is larger than that of the small gun, and hence the length of this shoulder signal is longer. This interpretation assumes that the shoulder signal is created by the small air bubble that is released prior to the main peak (shown by a yellow arrow in Figure 4). Furthermore, we notice that the average amplitude level of the shoulder signal is nearly doubled for the cluster signal (red line) compared to the single 300 cubic inch air gun (black line). The 70 cubic inch shoulder signal is slightly weaker than that for the 300 cubic inch air gun. Again this is interpreted to be caused by the larger upper chamber volume for the larger gun. The physical mechanism behind the shoulder signal can be multifold: First of all the escape of air from the upper chamber (or the top housing) will definitely create an acoustic signal (similar to when the air is released from the big, lower gun chamber). The escape of this air from the upper chamber is clearly shown in Figure 4 (marked by a yellow arrow in the top left photo). This tiny air bubble remains visible for the next three photos in Figure 4, and therefore it is likely to assume that this mini-bubble exists for several milliseconds, and that it will produce a weak acoustic signal. Second, as discussed in the previous section, water vapor cavities that are produced due to rapid water movements close to the air gun will collapse and create

high frequency signals. Other effects that might contribute to the shoulder signal are the solenoid (electric trigger mechanism for the air gun), the movement of the shuttle and vibrations caused by the shuttle movement.

There is one common feature for all the three signals shown in Figure 5 (bottom): The high frequency signal that occurs between 47 and 48 ms. I think this signal represents small cavities collapsing close to the air gun ports (as those shown in Figure 4). Since the size of these cavities are small, they will collapse within a fraction of a millisecond (equation 4), and therefore they will essentially “live” as long as the bubble velocity is above a certain threshold. Again, we observe that the magnitude of this potential cavitation signal is higher for larger guns. It is indeed very hard to prove that this signal is caused by collapsing cavities, and therefore I use the term “potential cavitation”. One way to further strengthen this hypothesis is to apply a high pass filter to the data and see if the very high frequencies survive or not. It is typical for cavitation signals that they show a strong high frequency content. This is shown in Figure 6, where a 30 kHz high pass filter has been applied, followed by taking the absolute value and a mild smoother. All signals show a distinct increase at approximately 47 ms, more pronounced for the big gun (black line) and the cluster (red line) than for the small gun (blue line). We also notice that the main peaks for this high frequency signal appears *prior* to the main peak for the unfiltered signatures: For the 70 cubic inch gun the main peak occurs at 48.5 ms and for the 300 cubic inch gun it is at 49.5 ms (Figure 5). For the high pass filtered data shown in Figure 6, these maxima occurs approximately 2 ms earlier. Furthermore, we notice that all three curves decay after the maximum, similar to the modeled bubble wall velocity shown in Figure 2 (bottom). All these observations support the hypothesis that the signal between 47 and 48 ms observed in Figure 5 is mainly caused by cavitation. It should also be stressed that this cavitation signal continues also after 48 ms, since we

observe high frequency signals above the background noise level in the time interval between 47 and 51 ms (Figure 6).

Another interesting observation that can be made from Figure 5 (bottom) is that the shoulder signal of the clustered air guns (red line) increases stepwise: The first step occurs at 44.0 ms and the next step at 44.4 ms. This is probably caused by a firing time delay of 0.4 ms between the two guns in the cluster. This is further strengthened by the fact that the shoulder signal of the cluster array is two times stronger than that of the single gun. After high pass filtering (Figure 6) we also observe a small time shift (0.2-0.3 ms) between the single gun (black line) and the cluster (red line).

VI. THE ECHO SOUNDER SIGNAL AND THE CAVITATION SIGNAL

The seismic vessel uses an echo sounder with a dominant frequency of 20 kHz. This signal is prominent if we apply a band pass filter (17.5 – 22.5 kHz) centered around the dominant frequency (Figure 7). We observe a periodic signal every 8 ms (approximately). However, the signal at 47 ms (marked by the blue arrow) is not caused by the echo sounder and is interpreted as cavitation signal from the air gun. Since the echo sounder signal definitely is a high frequency signal, we should try to isolate it as much as possible in the analysis. Figure 8 demonstrates how the echo sounder signal becomes more and more prominent as the frequency content of the recorded signal is increased. However, the interpreted cavitation signal around 47 ms is prominent for all frequencies and does not coincide with the echo sounder signal (Figure 7, bottom). This cavitation signal is further enhanced if several shots are stacked together prior to the analysis, as shown in Figure 9 where 4 shots from the single 300 cubic inch air gun have been aligned and then stacked prior to application of a 36-60 kHz band pass filter. The stacking procedure helps, since the echo sounder signals will arrive at random

times when different shots are stacked. When the 55 kHz high pass filtered data (red curve in Figure 9, bottom) is compared to the modeled velocity curve in Figure 2, we observe some similarities that may be used as a guide for a qualitative interpretation: As the air is pushed out of the air gun, the water velocity close to the ports reaches a maximum. At this maximum a high number of cavities is created close to the gun, and collapse almost instantaneously. As the velocity decreases, the number of cavities created decreases until the velocity is below the critical velocity (Equation 4). The width of the cavitation signal in Figure 9 (bottom) is approximately 2 ms. From the modeled velocity curve in Figure 2, this would correspond to a critical velocity of 45 m/s. We know that Figure 2 is not correct (it assumes spherical symmetry, does not include the air throttling through the ports etc. so this number is should only be used as an indication: It is indeed possible that the 55 kHz signal shown in Figure 9 is caused by cavitation.

VII. COMPARING SIGNATURES FROM A SINGLE GUN AND AN ARRAY OF 30 GUNS

Figure 10 shows a comparison between a 300 cubic inch single air gun and a full array (2730 cubic inches, 30 guns in total). We notice that the acoustic signal produced by the full array is significantly stronger (approximately 8.3 times) compared to the single 300 cubic inch gun. From the high pass filtered data (30 kHz high pass filter) we observe again a peak that occurs prior to the main peak of the signature, which is interpreted as being caused by small cavities collapsing close to the gun ports (shown in Figure 4). For the single gun, this event occurs as a clear peak. For the full array, we notice a more “bumpy” signal, indicating that various guns in the full array create cavities at different times depending on individual variation in firing times for the 30 guns in the array. We also notice that the primary peak signal of the full array (black line, top in Figure 10) is

actually composed of three individual peaks. These three peaks might be due to slight firing time delays between the three subarrays in the array. The size of the array is 12 by 15 m, yielding a diagonal of 19 m. For a hydrophone located 60 m away in the vertical direction, this might cause a difference in traveltime of approximately 2 ms. Therefore, the spread of the maximum peak of the full array might be caused by a combination of variation in gun firing time delays and small traveltime differences due to the areal spread of the array. Both these effects might therefore explain why we get this bumpy behavior of the high frequency cavitation signal occurring from approximately 47 to 54 ms for the full array (black curve in Figure 10, bottom): This high frequency signal is interpreted as being composed of individual cavities collapsing close to the gun ports.

The biggest difference between high pass filtered data for the full array and the single gun is however what occurs after 58 ms (Figure 10). A strong high frequency signal is gradually building up to a maximum occurring at approximately 65 ms, followed by a sudden decrease. This effect has been described previously by Landrø et al. (2011) and is denoted as ghost cavitation in Figure 10. We clearly see that it occurs after the strong negative signal around 57 ms. It is assumed that the collective effect of ghost signals from 30 individual guns arriving at approximately the same time (57 ms) and occurring at specific locations (above the mid array for instance) is sufficiently strong to lower the absolute pressure in the water close to zero, creating water vapor cavities. It is reasonable to assume that these cavities might be larger in size, and hence the collapse time (see equation 5) will be larger compared to the smaller cavities that collapse at the gun itself. The magnitude of the ghost cavitation signal is approximately 10 times larger than the high frequency signal associated with the main peak of the signature. Acoustic stimulation of cavities has been studied by numerous researchers. One early example was performed by Harrison (1952). He used a venture nozzle to

generated cavities by high speed motion of water from the nozzle (very similar to what I claim is the mechanism behind the cavities observed in Figure 4 in this paper). Plesset and Ellis (1955) demonstrated some years later that it is possible to create cavities by acoustic stimulation.

Figure 11 shows a broadband comparison (10 Hz to 62.5 kHz) of the amplitude spectra for the small air gun (70 cubic inch), the single 300 cubic inch air gun, the cluster and the full array. We notice that the full array is approximately 20 dB stronger than the other guns for the frequency range between 100 Hz up to 20 kHz. For frequencies between 20 and 60 kHz, the difference is somewhat less. For very low frequencies (close to 10 Hz) we notice that the curve for the smallest gun (70 cubic inch) crosses the larger gun (300 cubic inch). This cross over might be associated with the different bubble time period for the two signals: The 70 cubic inch gun has a bubble time period of 70 ms, corresponding to a resonance frequency of 14.3 Hz, while the 300 cubic inch gun has a bubble time period of 120 ms, corresponding to 8.3 Hz. Hence, the smaller gun will have maximum caused by the bubble oscillation for a frequency slightly above 10 Hz, while the bigger gun will have the maximum below 10 Hz. Another cause may simply be related to varying noise level between the shot series for the different gun configurations. Figure 12 shows noise records (taken from the 30 ms prior the actual firing of the source) for the four source configurations shown in Figure 11. We notice that the noise record corresponding to the 70 cubic inch air gun is above the other noise records, especially at the low frequency end. A comparison with an 1/f attenuation is also shown in this figure, and we notice that the decay is actually 1/f for frequencies between 10 Hz and 10 kHz. Above 10 kHz, the influence of the echo sounder signal is dominating. Figure 13 shows a comparison between the amplitude spectra of the nearest and furthest shot for the smallest air gun and the full array. We notice that the amplitude strength is practically equal for frequencies above 10 kHz for the single gun,

while the full array spectral difference reaches a maximum around 10-15 kHz and then slightly decreases. At the echo sounder frequency (20 kHz), we notice that there is a significant difference for the single gun spectrum (Figure 13). Again, this difference is mainly attributed to the strong ghost cavitation signal for the full array (which is stronger the nearer the source is). For the single gun, the cavitation signal is much weaker, and therefore drowning in the background high frequency noise.

Another way to demonstrate the significance of the ghost cavitation effect, is to add the signal recorded from the cluster array five times. The volume of the cluster array is 600 cubic inches, and by adding it 5 times and introducing random firing time delays between each of the 5 elements, a realistic signal simulating the effect of adding 5 clustered sources together (without accounting for the ghost cavitation effect) is achieved. The total volume of the full array is 2730 cubic inches, which is slightly less than 5 times 600 cubic inches. In Figure 14 we clearly see that although the strength of this synthetic 3000 cubic inch array is the same for low frequencies (less than 20-30 Hz), there is a significant gap between the full array and the 3000 cubic inch simulated result for frequencies above 100 Hz. It should be noted that some of the differences between the two arrays are not caused entirely by the ghost cavitation effect, since a more broadband frequency signal is obtained by simply using different source volumes. This is especially true for the frequency band between 20-100 Hz, where we observe that the full array has a better response compared to the synthetic array generated by summing the clustered air gun 5 times.

VIII. CONCLUSIONS

High speed photographs of a small air gun in a water tank show small bubbles attached to the gun itself that is interpreted as cavities. Simple modeling of the air being released from an air gun into the surrounding water shows that velocities might be well above critical velocity for cavity creation. A maximum water velocity of approximately 50 m/s is found by comparing two adjacent photos form the initial stages after the air gun has been fired. Recorded underwater acoustic signals, measured 60 m vertically below the air gun source, shows a high frequency signal (2-60 kHz) arriving prior to the main peak, which is interpreted as caused by collapsing cavities close to the gun. When the full array (30 air guns) is fired, an additional cavitation signal that is much stronger than the cavitation signals being produced by individual air guns is observed. This signal occurs at a later stage (after the ghost signal) and is referred to as ghost cavitation signal.

ACKNOLWLEDGMENTS

I thank the Norwegian Research Council for financial support to the ROSE consortium at NTNU. I acknowledge Jan Langhammer for creating the high speed photos of the air gun used in this paper, for numerous discussions on this topic and for critical review of the paper. ARCEx (Research Centre for Arctic Petroleum Exploration) is acknowledged for financial support.

REFERENCES

Amundsen, A., and M. Landrø, 2010, Seismic sources, part V, the hearing of marine mammals, GeoExpro, **7**, Vol. 6, 64-66.

Amundsen, A. and M. Landrø, 2011a, Seismic sources, part VI, high frequency signals from air guns, GeoExpro, **8**, Vol. 1, 69-71.

Amundsen, A. and M. Landrø, 2011b, Seismic sources, part VII, fish are big talkers, GeoExpro, **8**, Vol. 2, 64-67.

Barker, D. and M. Landrø, 2014, An alternative method for modeling close-range interactions between air guns, Geophysics, **79**, P1-P7.

Breitzke, M., O. Boebel, S. El Naggar, W. Jokat, and B. Werner, 2008, Broad-band calibration of marine seismic sources used by R/V Polarstern for academic research in polar regions, Geophys. J. Int., **174**, 505-524.

Coste, E., D. Gerez, H. Groenaas, O. P. Larsen, M. Wolfstirn, J. F. Hopperstad, R. Laws*, J. Norton, and M. Padula, 2014, Attenuated high-frequency emission from a new design of air-gun. SEG Technical Program Expanded Abstracts 2014, 132-137.

Dragoset, B., 2000, Introduction to air guns and air gun arrays, The Leading Edge **19**, 892-897.

Goold, J.C. and P. J. Fish, 1998, Broadband spectra of seismic survey air-gun emissions, with reference to dolphin auditory thresholds, J. Acoust. Soc. Am., **103,** 2177-2184.

Groenaas, H.S.G., S.A. Frivik, A.S. Melboe and M. Svendsen, 2011, A novel marine mamal monitoring system utilizing the seismic streamer spread, 73rd EAGE Meeting, Expanded Abstracts, D047.

Harrison, M., 1952, An experimental study of single bubble cavitation noise, The Journal of the Acoustical Society of America, **24**, 776-782.

Landrø, M., 1992, Modelling of GI gun signatures, Geophysical Prospecting, **40**, 721-747.

Landrø, M., G. Zaalberg-Metselaar, B. Owren, and S. Vaage, 1993, Modeling of water-gun signatures, Geophysics, **58**, 101-109.

Landrø, M., L. Amundsen and D. Barker, 2011, High-frequency signals from air-gun arrays, Geophysics, **76**, Q19-Q27.

Landrø, M., L. Amundsen and J. Langhammer, 2013, Repeatability issues of high-frequency signals emitted by air-gun arrays, Geophysics, **78**, P19-P27.

Langhammer, J., 1994, Experimental studies of energy loss mechanisms in air gun bubble dynamics, PhD thesis, NTH 1994:125.

Langhammer, J. and M. Landrø, 1996, High speed photography of the bubble generated by an air gun, Geophysical Prospecting, **44**, 153-173.

Plesset, M.S. and A. T. Ellis, 1955, On the mechanism of cavitation damage, Trans. ASME, 1054-1064.

Rayleigh, O. M., 1917, On the pressure developed in a liquid during the collapse of a spherical cavity, Phil. Mag., **34**, 94-98.

Ziolkowski, A., 1970, A method for calculating the output pressure waveform from an air gun, Geophysical Journal of the Royal Astronomical Society, **21**, 137-161.

FIGURE CAPTIONS

Figure 1: Photo of a small Bolt air gun showing the main chamber (lower chamber) that is initially filled with compressed air, the upper chamber, the four ports and the shuttle that moves rapidly upwards when the gun is fired.

Figure 2: Modeled bubble radius (top) and bubble wall velocity (bottom) versus time for a 70 (solid line) and a 300 (dashed line) cubic inch air gun. These results are obtained by numerical solution of equation 1 (Rayleigh equation) assuming a source depth of 5 m, and that the initial bubble pressure is 137 bar. As expected, both maximum radius and bubble time period increases with increasing gun volume. In this case, the maximum bubble wall velocity is practically equal for the two gun volumes.

Figure 3: Modeling air escaping through the ports of an air gun using equation 3. Parameters used: A=0.0005 m^2 (port area), m=0.25 kg ("piston mass"), gamma = 1.4, p0=137 bar z_s=5 m. The larger gun achieves higher water velocity compared to the small gun, indicating higher probability for cavity creation.

Figure 4: High speed photos of a 600 Bolt air gun in a water tank. To the left we see that some air has been released from the upper chamber (small air bubble marked with a yellow arrow). On the next photo (b) the air from the main chamber (lower chamber) starts to escape through the ports, and on the last photo (d) we clearly see four bubbles (corresponding to the four ports of the gun) that will merge into one big bubble some milliseconds later. Photos from Jan Langhammer's PhD work, 1991.

Figure 5: Top: Unfiltered signatures of a single 70 cubic inch air gun (blue line), a single 300 cubic inch air gun (black line) and a cluster of two 300 cubic inch air guns (red line). Bottom: Zoom of the top figure showing the shoulder signal (44-48 ms). Notice that the "shoulder signal" is longer for the 300 cubic inch air gun(s) compared to the 70 cubic inch air gun.

Figure 6: High pass (30 kHz) filtered signatures, followed by absolute value and smoothing of a single 70 cubic inch air gun (blue line), a single 300 cubic inch air gun (black line) and a cluster of two 300 cubic inch air guns (red line). Notice that there is a significant increase in high frequency signal at approximately 47 ms for all signatures.

Figure 7: One shot record filtered with a 17.5-22.5 kHz band pass filter. The regular peaks (interval approximately 8 ms) are the echo sounder signal. Note that the peak at 47 ms (marked by the blue arrow) is *not* caused by the echo sounder, but the clustered air gun in this case (corresponding to the red peak in Figure 6).

Figure 8: Signature of the 300 cubic signatures filtered with various filters: No filter (black), 2-10 kHz (red), 10-15 kHz (blue), 18-22 kHz (purple), 30-60 kHz (green). The dominant frequency of the echo sounder is 20 kHz, and hence we see the regular peaks (approximately 8 ms interval) on the purple curve. Notice that the signal prior to the main peak is observed for ALL frequencies (see zoomed version below). Scaling applied to the various curves: 2-10 kHz: 82; 10-15 kHz: 185; 18-22 kHz: 269 and 30-60 kHz: 478. Bottom: Zoomed version of the same figure.

Figure 9: Top: Four shots of a single 300 cubic inch air gun. Bottom: Stack of the four shots after application of a 2 kHz (black curve) and a 55 kHz (red curve) high pass filter. The filtering process is followed by absolute value (of each time sample) and a gentle smoother.

Figure 10: Top: Recorded far field signals of full array (black) and 300 cubic inch single air gun (red). The data have been normalized prior to plotting (the maximum amplitude of the full array is 8.3 times that of the single gun). Bottom: Same data after applying a 30 kHz high pass filter, absolute value and smoothing. Notice that cavitation signals are observed prior to the main peak for the single gun (marked by red arrow), and after the ghost signal for the full array, denoted as ghost cavitation. The ghost cavitation signal is approximately 10 times stronger than the high frequency signal observed around 50 ms for the full array.

Figure 11: Amplitude spectra in dB for the full array (black line), the 70 cubic inch air gun (blue line), the 300 cubic inch air gun (green line) and the 2x300 cubic inch cluster (red line). The peak around 20 kHz for the three latter curves is caused by the echo sounder of the vessel. Notice that the difference between the full array and the single guns is of the order of 20 dB for frequencies between 100 Hz and 20 kHz.

Figure 12: Noise spectra for the 4 shots used in the previous figure. A window of 30 ms prior to the gun firing time is used for the analysis. We notice that the noise level is higher prior to the firing of the 70 cubic inch gun (blue line) compared to the others. We notice the characteristic peak of the echo sounder signal at 20 kHz. The slope of this noise corresponds approximately to 1/f attenuation between 100 Hz and 7 kHz.

Figure 13: Comparison of the nearest (black lines) and furthest (red lines) shots for the single 70 cubic inch air gun (top) and the full array (bottom). Notice the significant differences between the two sources, especially for frequencies above 10 kHz.

Figure 14: Amplitude spectrum of full array (black) and the 2 gun cluster (red). The blue line represent the 2 gun cluster signal being summed 5 times using a random time delay (1-3 ms) between the 5 “shots” prior to summation. Notice that the “stacked” cluster array has similar amplitudes compared to the full array for frequencies less than 30 Hz. For higher frequencies the discrepancy between the two curves increases up to 20 kHz.

FIGURES

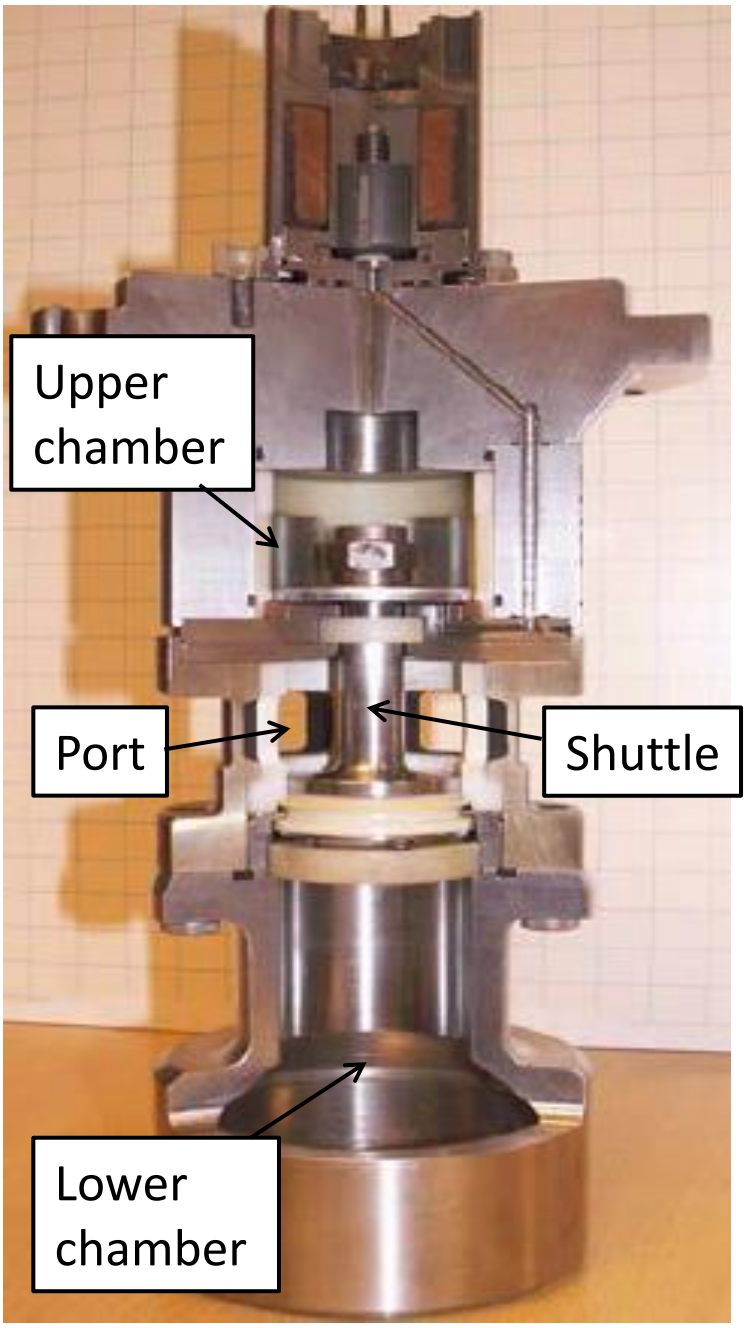


Figure 1: Photo of a small Bolt air gun showing the main chamber (lower chamber) that is initially filled with compressed air, the upper chamber, the four ports and the shuttle that moves rapidly upwards when the gun is fired.

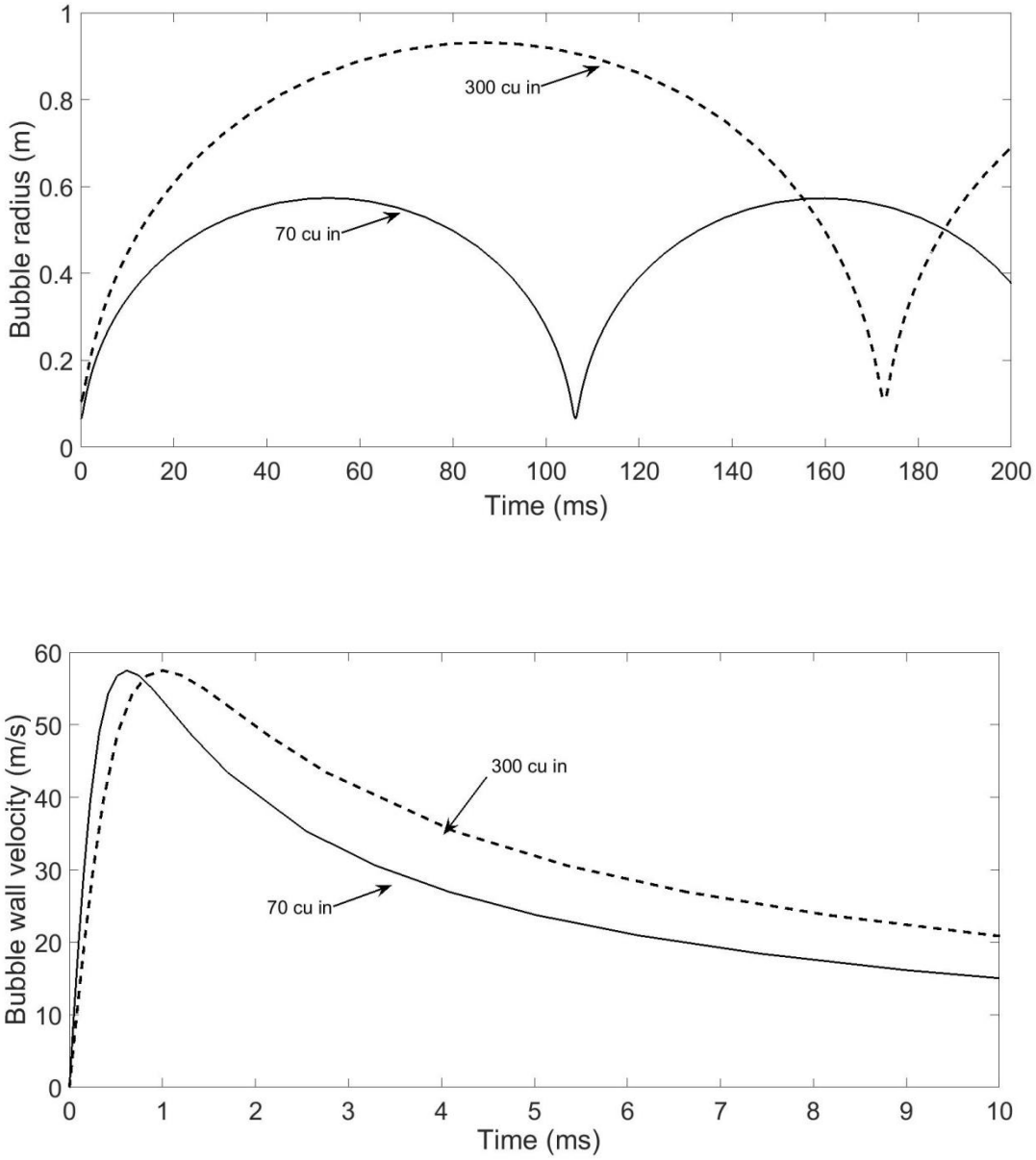


Figure 2: Modeled bubble radius (top) and bubble wall velocity (bottom) versus time for a 70 (solid line) and a 300 (dashed line) cubic inch air gun. These results are obtained by numerical solution of equation 1 (Rayleigh equation) assuming a source depth of 5 m, and that the initial bubble pressure is 137 bar. As expected, both maximum radius and bubble time period increases with increasing gun volume. In this case, the maximum bubble wall velocity is practically equal for the two gun volumes.

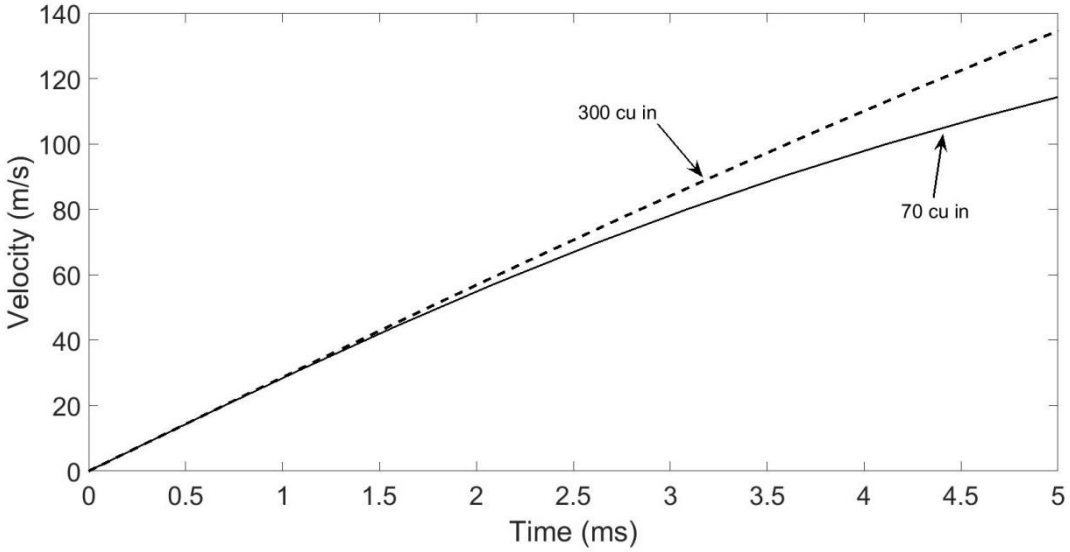


Figure 3: Modeling air escaping through the ports of an air gun using equation 3. Parameters used: A=0.0005 m^2 (port area), m=0.25 kg (“piston mass”), gamma = 1.4, p0=137 bar z_s=5 m. The larger gun achieves higher water velocity compared to the small gun, indicating higher probability for cavity creation.

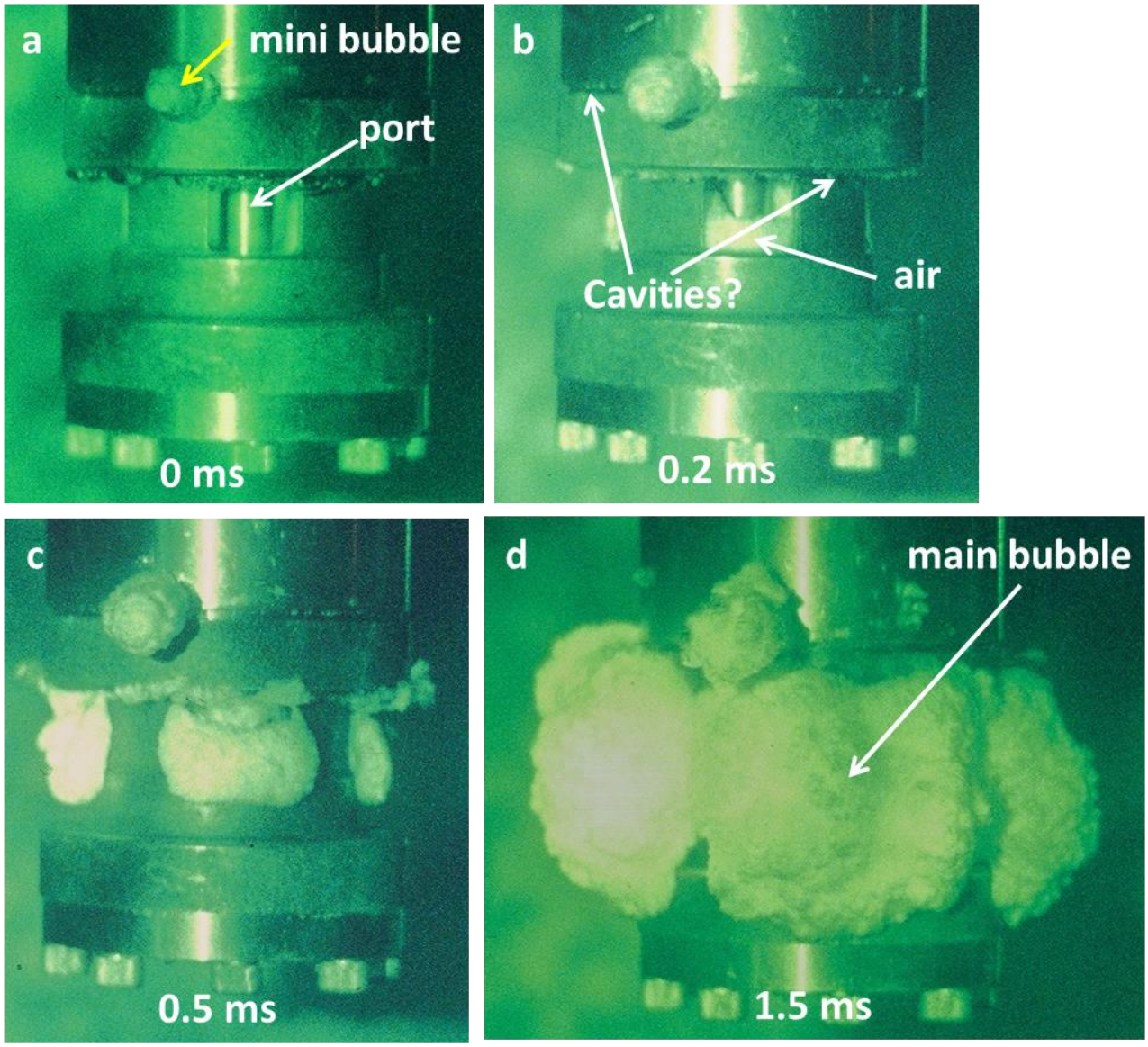


Figure 4: High speed photos of a 600 Bolt air gun in a water tank. To the left we see that some air has been released from the upper chamber (small air bubble marked with a yellow arrow). On the next photo (b) the air from the main chamber (lower chamber) starts to escape through the ports, and on the last photo (d) we clearly see four bubbles (corresponding to the four ports of the gun) that will merge into one big bubble some milliseconds later. Photos from Jan Langhammer's PhD work, 1991.

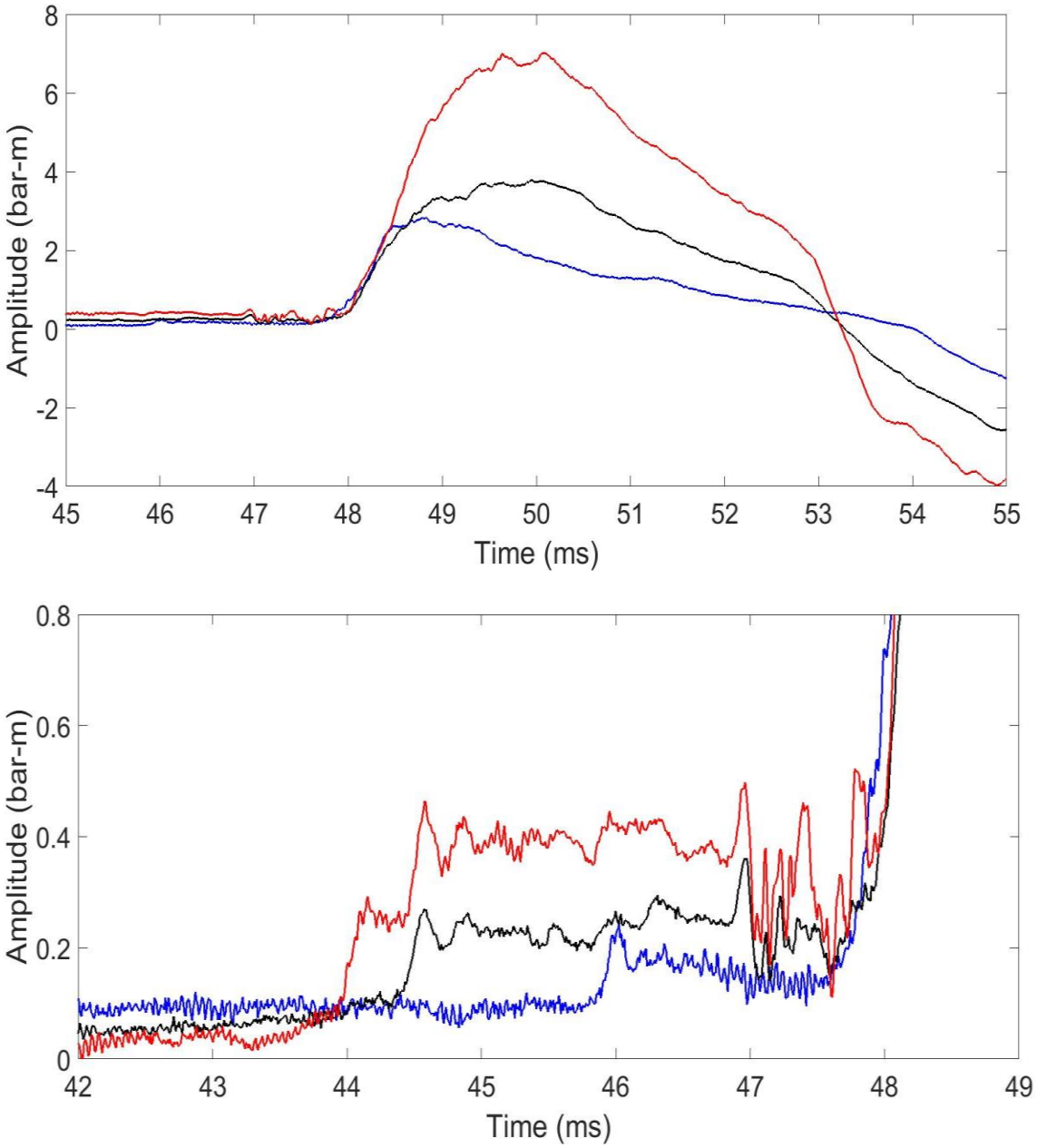


Figure 5: Top: Unfiltered signatures of a single 70 cubic inch air gun (blue line), a single 300 cubic inch air gun (black line) and a cluster of two 300 cubic inch air guns (red line). Bottom: Zoom of the top figure showing the shoulder signal (44-48 ms). Notice that the "shoulder signal" is longer for the 300 cubic inch air gun(s) compared to the 70 cubic inch air gun.

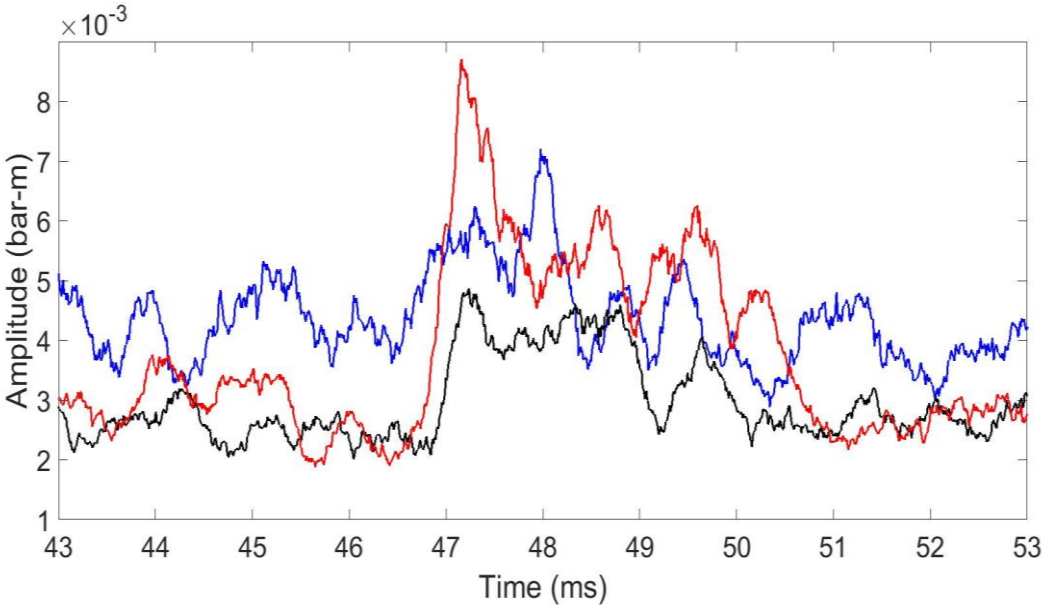


Figure 6: High pass (30 kHz) filtered signatures, followed by absolute value and smoothing of a single 70 cubic inch air gun (blue line), a single 300 cubic inch air gun (black line) and a cluster of two 300 cubic inch air guns (red line). Notice that there is a significant increase in high frequency signal at approximately 47 ms for all signatures.

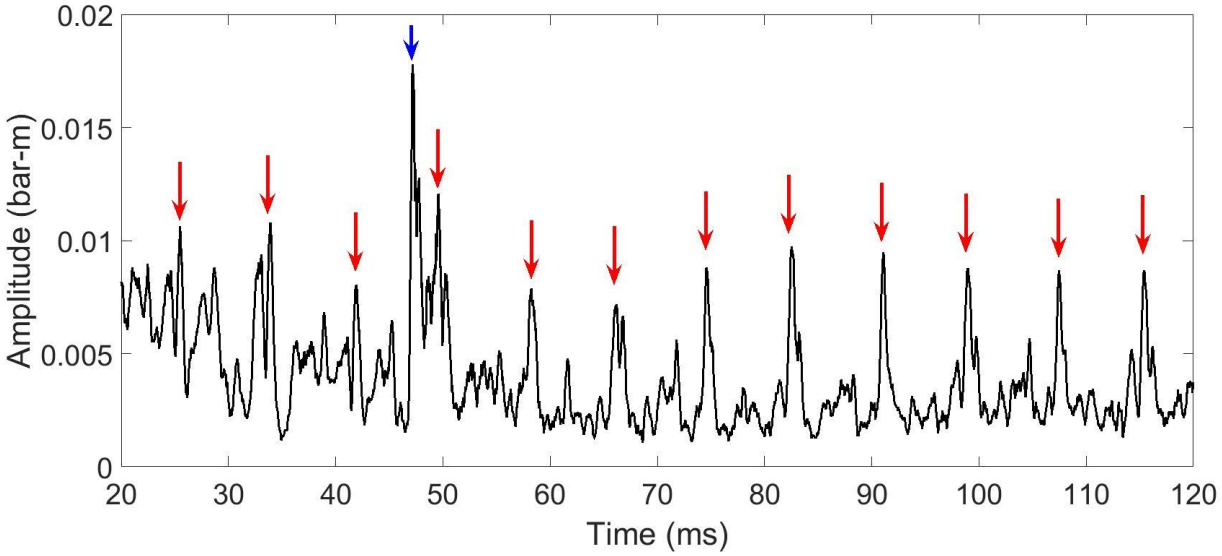


Figure 7: One shot record filtered with a 17.5-22.5 kHz band pass filter. The regular peaks (interval approximately 8 ms) are the echo sounder signal. Note that the peak at 47 ms (marked by the blue arrow) is *not* caused by the echo sounder, but the clustered air gun in this case (corresponding to the red peak in Figure 6).

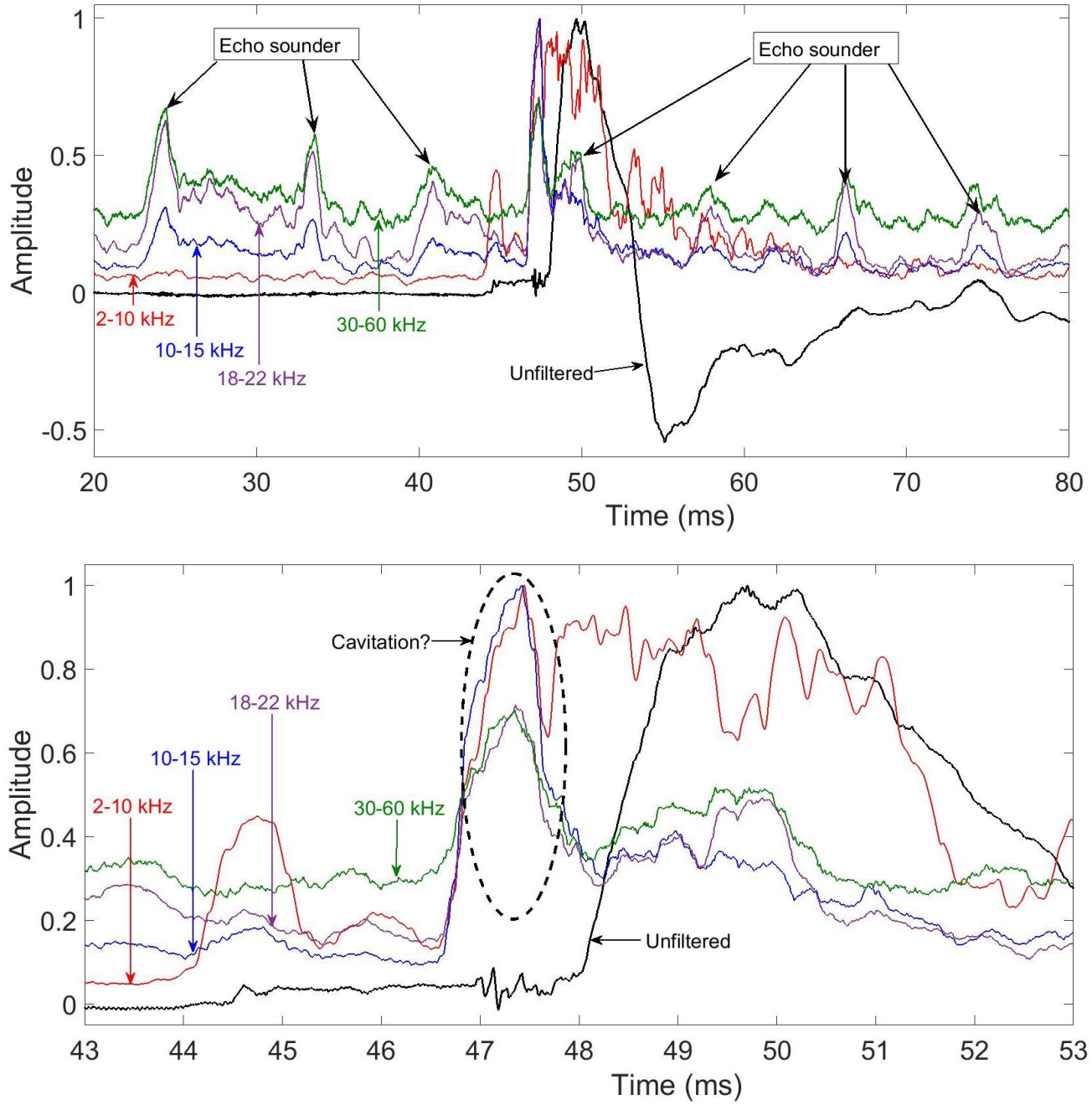


Figure 8: Signature of the 300 cubic signatures filtered with various filters: No filter (black), 2-10 kHz (red), 10-15 kHz (blue), 18-22 kHz (purple), 30-60 kHz (green). The dominant frequency of the echo sounder is 20 kHz, and hence we see the regular peaks (approximately 8 ms interval) on the purple curve. Notice that the signal prior to the main peak is observed for ALL frequencies (see zoomed version below). Scaling applied to the various curves: 2-10 kHz: 82; 10-15 kHz: 185; 18-22 kHz: 269 and 30-60 kHz: 478. Bottom: Zoomed version of the same figure.

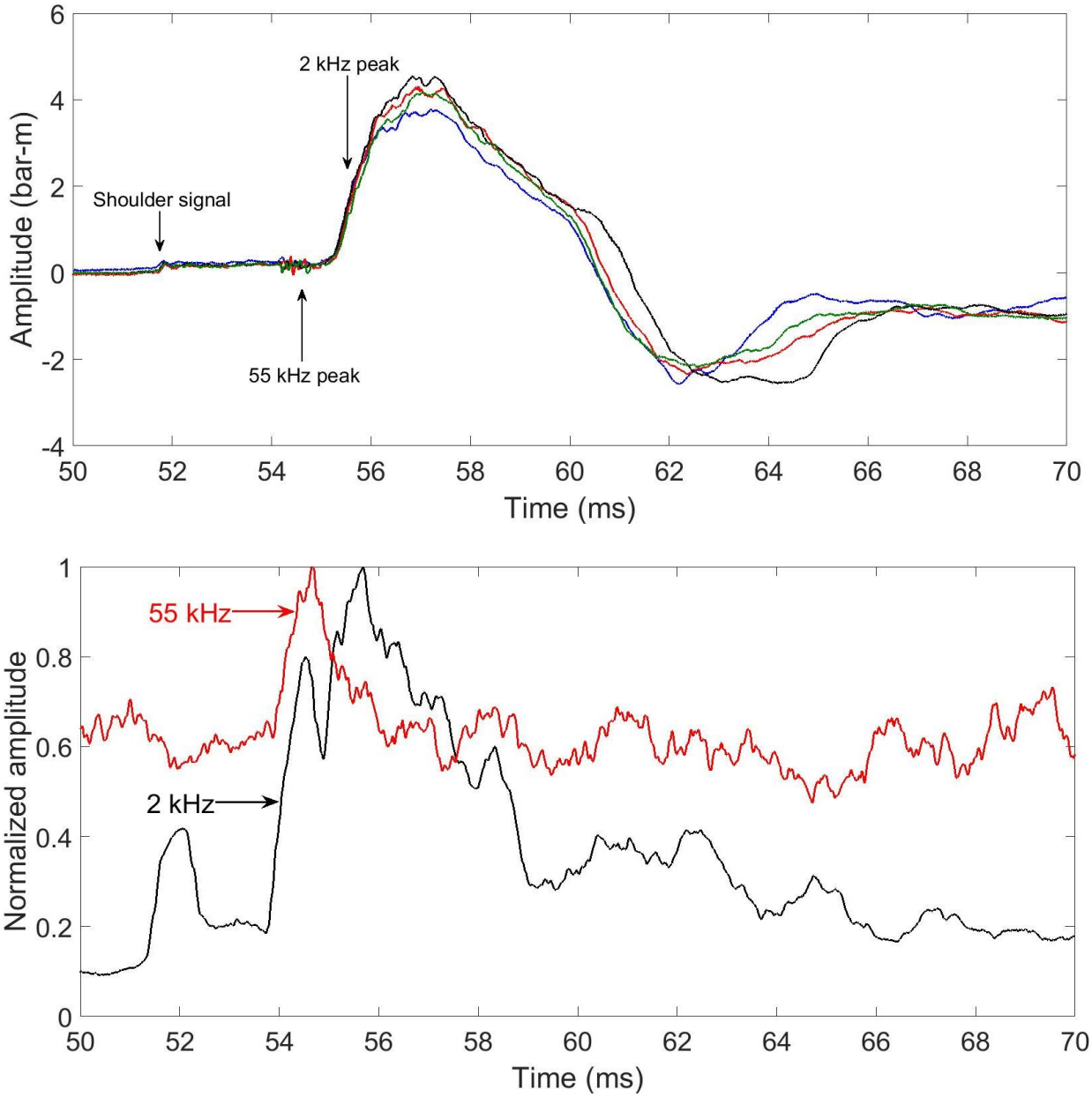


Figure 9: Top: Four shots of a single 300 cubic inch air gun. Bottom: Stack of the four shots after application of a 2 kHz (black curve) and a 55 kHz (red curve) high pass filter. The filtering process is followed by absolute value (of each time sample) and a gentle smoother.

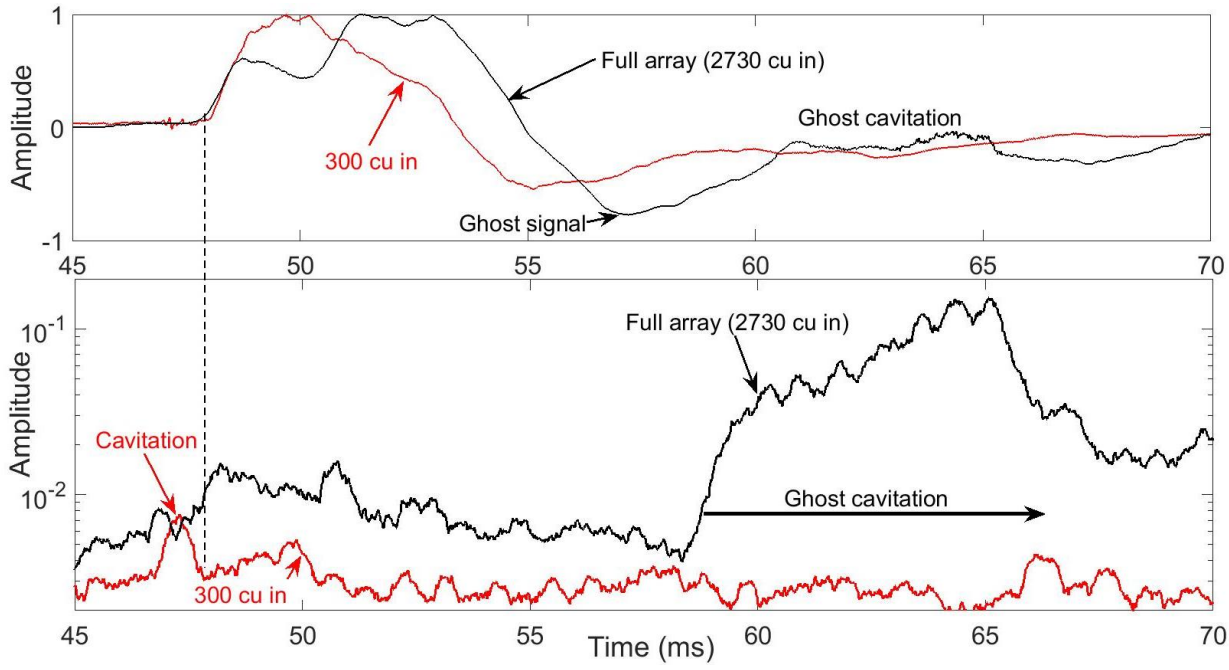


Figure 10: Top: Recorded far field signals of full array (black) and 300 cubic inch single air gun (red). The data have been normalized prior to plotting (the maximum amplitude of the full array is 8.3 times that of the single gun). Bottom: Same data after applying a 30 kHz high pass filter, absolute value and smoothing. Notice that cavitation signals are observed prior to the main peak for the single gun (marked by red arrow), and after the ghost signal for the full array, denoted as ghost cavitation. The ghost cavitation signal is approximately 10 times stronger than the high frequency signal observed around 50 ms for the full array.

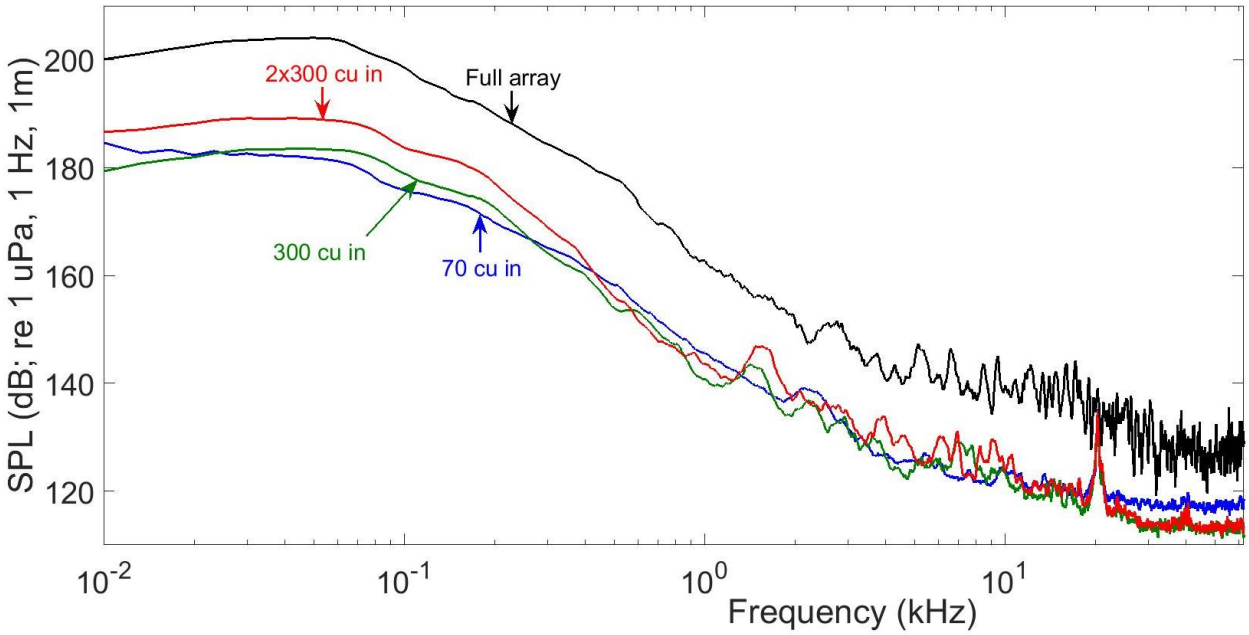


Figure 11: Amplitude spectra in dB for the full array (black line), the 70 cubic inch air gun (blue line), the 300 cubic inch air gun (green line) and the 2x300 cubic inch cluster (red line). The peak around 20 kHz for the three latter curves is caused by the echo sounder of the vessel. Notice that the difference between the full array and the single guns is of the order of 20 dB for frequencies between 100 Hz and 20 kHz.

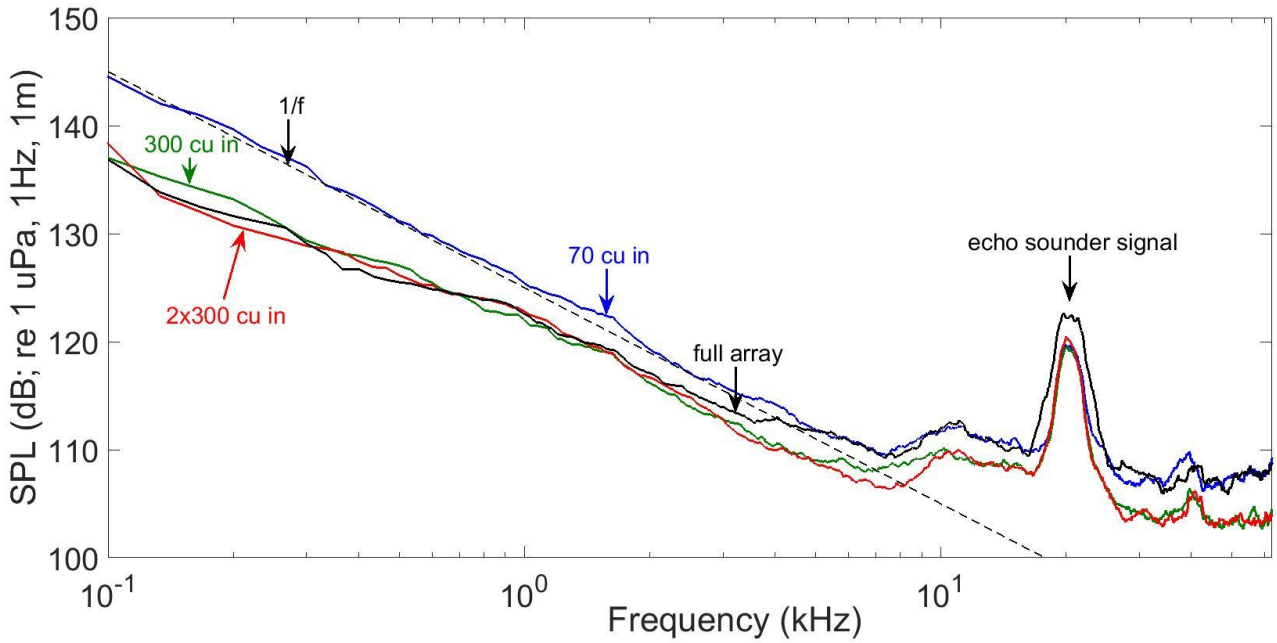


Figure 12: Noise spectra for the 4 shots used in the previous figure. A window of 30 ms prior to the gun firing time is used for the analysis. We notice that the noise level is higher prior to the firing of the 70 cubic inch gun (blue line) compared to the others. We notice the characteristic peak of the echo sounder signal at 20 kHz. The slope of this noise corresponds approximately to 1/f attenuation between 100 Hz and 7 kHz.

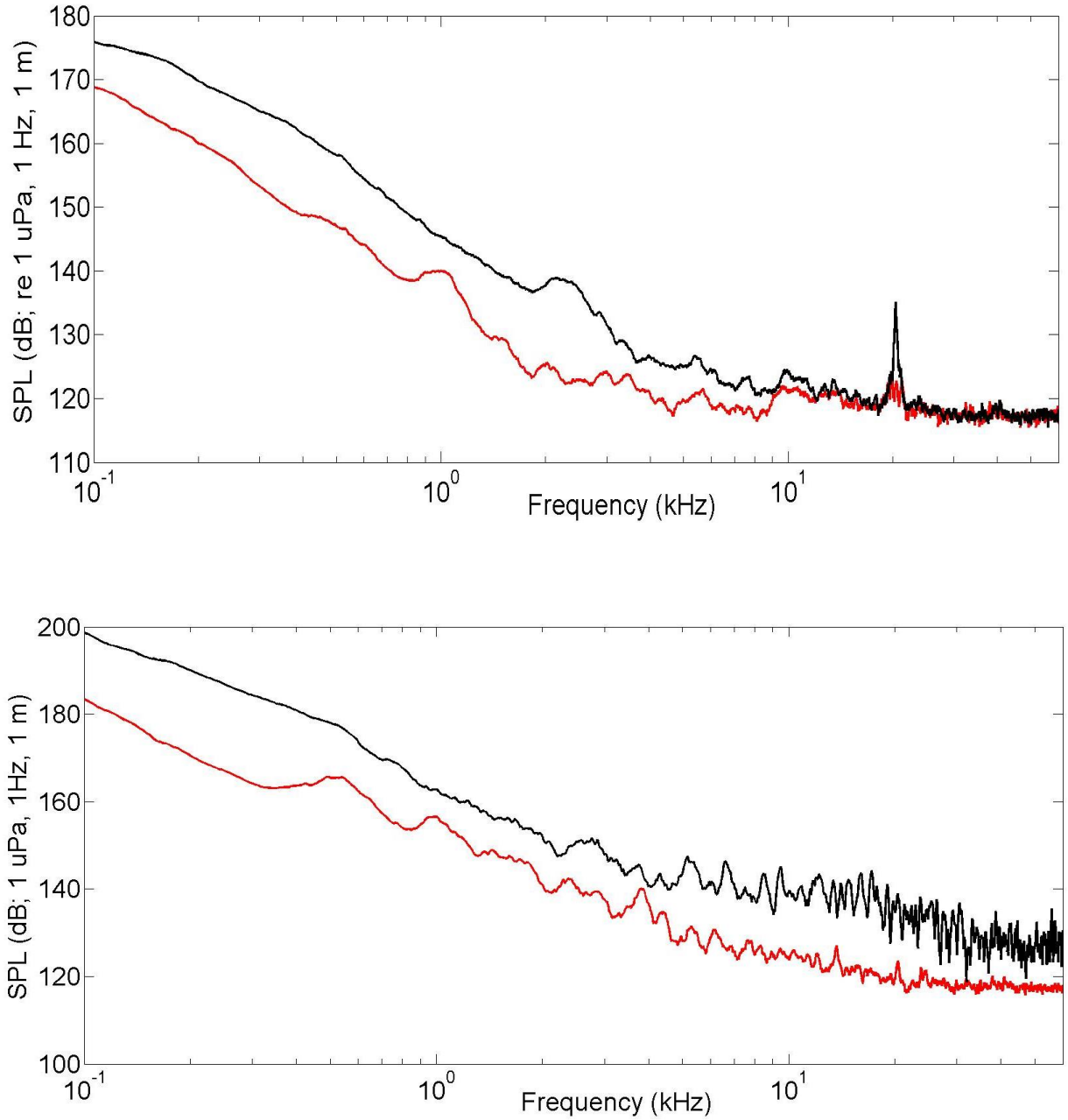


Figure 13: Comparison of the nearest (black lines) and furthest (red lines) shots for the single 70 cubic inch air gun (top) and the full array (bottom). Notice the significant differences between the two sources, especially for frequencies above 10 kHz.

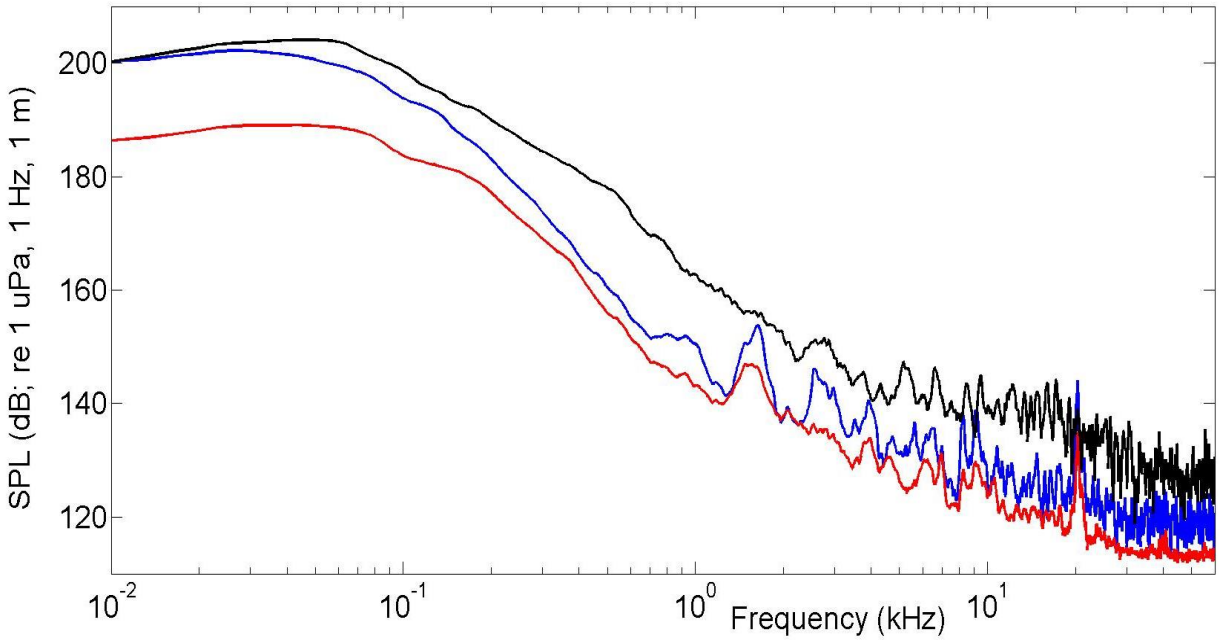


Figure 14: Amplitude spectrum of full array (black) and the 2 gun cluster (red). The blue line represent the 2 gun cluster signal being summed 5 times using a random time delay (1-3 ms) between the 5 “shots” prior to summation. Notice that the “stacked” cluster array has similar amplitudes compared to the full array for frequencies less than 30 Hz. For higher frequencies the discrepancy between the two curves increases up to 20 kHz.